Microbial Biotechnology

WILEY

MICROBIAL BIOTECHNOLOGY Open Access

RESEARCH ARTICLE OPEN ACCESS

Rational Design Assisted by Evolutionary Engineering Allows (De)Construction and Optimization of Complex Phenotypes in *Pseudomonas putida* KT2440

Blas Blázquez[1,2] | Juan Nogales[1,2,3]

[1]Department of Systems Biology, Centro Nacional de Biotecnología CSIC, Madrid, Spain | [2]CNB DNA Biofoundry (CNBio), CSIC, Madrid, Spain | [3]Interdisciplinary Platform for Sustainable Plastics Towards a Circular Economy-Spanish National Research Council (SusPlast-CSIC), Madrid, Spain

Correspondence: Juan Nogales (jnogales@cnb.csic.es)

Received: 15 November 2024 | **Revised:** 3 March 2025 | **Accepted:** 5 March 2025

Funding: This research received funding from the European Union's Horizon 2020 research and innovation programme under grant agreement numbers 814650 (SynBio4Flav), 870294 (MIX-UP) and 101000733 (PROMICON), as well as the TED2021-130689B-C33 (SyCoSys) and PID2022-139247OB-I00 (Rob3D) projects funded by MCIN/AEI/10.13039/501100011033 and European Union (Next Generation EU/PRTR) funding, a way to make Europe.

Keywords: complex phenotype | fitness landscape | GENIO | genome expansion | metabolic engineering | *Pseudomonas putida*

ABSTRACT

Beyond the rational construction of genetic determinants to encode target functions, complex phenotype engineering requires the contextualisation of their expression within the metabolic and genetic background of the host strain. Furthermore, wherever metabolic complexity is involved, phenotype engineering demands standard, reliable, plug-and-play tools. We introduce GENIO (GENome Integration and fitness Optimization platform for *Pseudomonas putida*), a framework to optimise genetic circuit performance by means of (i) chromosome-location-based differential gene expression and (ii) subsequent fitness improvement through evolutionary engineering if needed. Using gene expression strength and cell-to-cell variation, we characterised 10 *P. putida* chromosomal loci (ppLPS) to show that genome context rather than distance to ORI is the main factor driving differential expression performance. We further contextualised ppLPS gene expression against well-known chromosomal integration sites and plasmids displaying different copy numbers. GENIO supports comprehensive exploration of the gene expression space across *P. putida*'s genome while unlocking performance optimization of complex heterologous metabolic pathways through evolutionary engineering. To demonstrate the usability of GENIO, we restored *P. putida*'s aromatic hydrocarbon metabolism by (de)constructing the toluene/*m*-xylene catabolic pathway coded in the pWW0 plasmid. We also showed that engineering complex phenotypes requires accurate contextualisation of the synthetic pathways involved, a process that benefits from biological robustness.

1 | Introduction

The soil bacterium *Pseudomonas putida*, particularly the KT2440 strain, is a premier chassis in the field of metabolic engineering and synthetic biology (Martínez-García and de Lorenzo 2024). Known for its remarkable adaptability and robustness (Belda et al. 2016), *P. putida* offers several advantages that make it a preferred host for a variety of biotechnological applications, including industrial biotransformation and environmental remediation (Weimer et al. 2020). One of the most compelling reasons for using *P. putida* KT2440 is its versatile metabolism, which allows it to thrive in changing and often harsh environments (Manoli et al. 2022). This bacterium can metabolise a wide range of substrates, making it highly adaptable to different bioprocesses (Jimenez et al. 2002). Its robust redox metabolism is particularly beneficial for reactions

requiring strong oxidising or reducing conditions, which are often challenging for other microbial platforms (Ebert et al. 2011). Another critical attribute of *P. putida* KT2440 is its tolerance to physicochemical stress. This resilience is essential for maintaining the stability and efficiency of engineered pathways under industrial operating conditions (Nikel et al. 2014).

The availability of advanced system biology (Nogales et al. 2020) and molecular tools for genetic manipulation (Torres-Bacete et al. 2021; Kozaeva et al. 2024) has further enhanced the appeal of *P. putida* KT2440 as a synthetic biology chassis (Martínez-García and de Lorenzo 2024). Researchers have developed many tools for accurate genetic editing to enable integration and expression of complex metabolic pathways. Such tools include replicative plasmids, site-specific recombinases, transposon mutagenesis, recombineering techniques and CRISPR-Cas systems (Cook et al. 2018; Martin-Pascual et al. 2021). These capabilities have opened new avenues for biotechnological innovations, including the production of high-value chemicals, bioplastics and compounds with pharmaceutical applications (Nikel and de Lorenzo 2018).

Genomic editing tools for *P. putida* have revolutionised our ability to explore cellular fitness and generate diverse phenotypes. Fitness landscape refers to the relationship between an organism's phenotype (observable traits) and its genotype (genetic makeup). Among other factors, the concentration of enzymes from synthetic genetic circuits plays a key role in influencing cellular fitness. This is crucial for maintaining a balanced metabolic state and is dependent on the host (Tas et al. 2021). Indeed, optimal fitness requires an enzymatic Goldilocks balance, that is, a situation where enzyme concentrations are neither too low nor too high (Agozzino et al. 2020). Insufficient enzyme levels result in low metabolic flux and hinder a cell's ability to perform specific tasks. Conversely, excessively high enzyme concentrations lead to energy wastage and make the cell less competitive compared to other more energetically optimised cells (Eames and Kortemme 2012). Genome editing tools enable accurate modification of genes and/or regulatory elements, so it is possible to control gene functions and metabolic pathways to support cellular adaptation to changing environmental conditions and metabolic challenges. Such tools facilitate the rational engineering of metabolic pathways, so ramping up their level of sophistication is critical to tackling increasingly complex projects successfully.

Complex phenotype engineering endeavours often demand a coupling of rational design and evolutionary engineering (Dragosits and Mattanovich 2013; Sauer 2001). Evolutionary approaches to engineer bacteria have proved themselves as a powerful tool to drive changes in fitness (positive or negative), thus reflecting the dynamic interplay between genetic variation and environmental pressures (Acerenza 2016). When bacteria are exposed to a specific selection pressure, such as an antibiotic or a nutrient-limited environment, mutations that confer a survival advantage are more likely to be propagated. These advantageous mutations enhance the bacteria's fitness in a particular context, allowing them to outcompete less adapted strains (Denamur and Matic 2006). However, this gain in fitness is often context-dependent, and mutations that enhance survival under one set of conditions may be detrimental under different circumstances. For instance, antibiotic resistance can incur a metabolic cost, slowing growth rates when the antibiotic is absent (Andersson and Hughes 2010; Melnyk et al. 2015). Similarly, bacteria might lose non-essential genes that are costly to maintain under specific conditions, resulting in a streamlined genome that enhances fitness in a given niche but reduces versatility in other environments (Helsen et al. 2020).

Aside from the variability of tools for genome modification, full exploitation of *P. putida*'s potential relies on the development of standardised, plug-and-play and high-throughput genome editing techniques. In this regard, recent studies have identified and characterised novel sites of genomic integration (Chaves et al. 2020; Köbbing et al. 2024). In this context, we present GENIO (GENome Integration and fitness Optimization platform for *Pseudomonas putida*) a novel synthetic biology tool (synbiotool) that presents several advantages with respect to previous efforts. Specifically: (i) GENIO is a library of vectors based on the SEVA architecture (a sibling of pSEVA) containing integration loci uniformly distributed across the *P. putida* chromosome; (ii) its integration process preserves the functional structure of *P. putida*'s chromosome, avoiding coding sequences; and (iii) the expression from its specific Landing Pad Sequences (LPSs) has been fully calibrated in terms of expression strength using both cis and trans reference systems. Moreover, GENIO offers a dual optimisation strategy for genetic circuits, leveraging differential expression at different chromosomal loci and evolutionary improvement of cell fitness by navigating local crests and troughs until optimal peaks are found. In our research, we deconstructed the toluene/*m*-xylene catabolic pathway cluster (a complex system comprising 21 genes organised into three gene clusters, including two large catabolic operons (8.5 and 11.5 kb) and a complex regulatory module (3.1 kb) from the pWW0 plasmid) and reconstructed it at specific locations in *P. putida* KT2440's chromosome. Using GENIO, we were able to demonstrate successful adaptation of *P. putida* through the incorporation of new genetic material coupled to adaptive evolution. GENIO supports exploration of different spatial arrangements within the cell to achieve optimal performance of the toluene metabolism.

2 | Materials and Methods

2.1 | Bacterial Strains, Growth Conditions and Genetic Constructs

Bacterial strains and plasmids used in this study are presented in Table S1. *Escherichia coli* cells cultivated at 37°C in lysogenic broth (LB) medium were used as hosts for cloning and screening procedures. For solid cultivation, 1.5% (w/v) agar was added to the medium. *Pseudomonas putida* cells were cultivated at 30°C in M9 minimal medium (Abril et al. 1989) supplemented with 2 mM MgSO4, 1× goodies and 34 μM EDTA. 20 mM glucose, 6 mM toluene and 5 mM *m*-xylene were used as carbon sources. When needed, kanamycin (Km) 50 $\mu g\,mL^{-1}$, ampicillin (Ap) 100 $\mu g\,mL^{-1}$, chloramphenicol (Cm) 30 $\mu g\,mL,^{-1}$ and gentamycin (Gm) 10 $\mu g\,mL^{-1}$ for *E. coli* and 20 $\mu g\,mL^{-1}$ for *P. putida* were added to the growth media.

LPS DNA parts were synthesized by GenScript Biotech Corporation and cloned into the pSEVA611 vector using AscI-SanDI restriction enzyme sites. LPS sequences used in ppLPS plasmids were cleaned of restriction enzyme sites present in the pSEVA backbone while maintaining codon usage for *P. putida*.

The heterologous DNA pem7-GFP from plasmid pSEVA2313G (https://seva-plasmids.com/find-your-plasmid/) was cloned into the cargo of the pTn7-M vector and the suicide plasmids ppLPS (ppLPS1 to 10) using the restriction sites available in the MCS. pem7GFP was digested with PacI and SpeI, and the gel-purified fragment was ligated into the ppLPS vectors. The resulting plasmids were named ppLPS1 pem7GFP, ppLPS2 pem7GFP and so on until ppLPS10 pem7GFP (Table S1). Sequencing with primers L3S5 and ECK3 was used to verify the integrity of the new constructions.

Operons from the toluene/*m*-xylene cluster were amplified from *P. putida* mt-2 by colony PCR. Primers xylR3 and xylS3 were used to amplify the xylRS regulatory node as a 3218 base pair (bp) PacI/SpeI fragment. The Upper operon was amplified as an 8486 bp PacI/KpnI fragment with primers upper5 and upper3. Finally, the Meta operon was amplified as two separate fragments: fragment 5969 bp PacI/BsrGI was amplified with primers meta5 and BsrGmeta3, and fragment 5609 bp BsrGI/SpeI was amplified with primers BsrGmeta5 and meta3. Clusters were cloned into different ppLPS vectors (Table S2).

Golden Standard (Blázquez et al. 2023) was used to assemble transcriptional units (TUs) carrying a BG17 promoter, RBS consensus, *yfp* or *rfp* reporter genes, and a T500 terminator. TUs were subcloned into a pTn7-M vector and integrated in the *attTn7* region of strains mt-2 and SBG1084 (Table S1).

Plasmids and DNA were PCR-amplified with oligonucleotides purchased from Sigma–Aldrich (Table S3) and purified with NZYkits supplied by NZYtech. DNA templates for colony PCR assays were obtained by picking a single fresh colony from an agar plate and transferring it to a PCR reaction tube. BLAST (https://blast.ncbi.nlm.nih.gov/Blast.cgi) was used to check DNA sequences against the Pseudomonas Genome Database (http://www.pseudomonas.com).

2.2 | Genome Editing in *Pseudomonas putida*

ppLPS vectors were integrated into the chromosome at target locations using *P. putida*'s native homologous recombination mechanism (a full description is provided in the Supporting Information). pTn7 vectors were transferred by conjugation following a previously described protocol (Zobel et al. 2015).

2.3 | Flow Cytometry Assay

Overnight cultures of *P. putida* in M9 minimal medium supplemented with 20 mM glucose were inoculated into 20 mL of fresh medium at 0.1 OD_{600} and grown for 3–5 h in an orbital shaker set to 30°C and 220 rpm. When cultures reached the exponential phase (0.4–0.6 OD_{600}), they were diluted in filtered PBS and immediately subjected to flow cytometer analysis using a MACSQuant VYB cytometer (Miltenyi Biotec, Bergisch Gladbach, Germany). GFP was excited at 488 nm and the fluorescence signal was recovered with a 525 ± 40 nm band-pass filter. RFP was excited at 530 nm and the fluorescence signal was recovered with a 580 nm band-pass filter. The assay was run with two biological replicates, and 50,000 events gated by forward scatter height (FSC-H) and side scatter height (SSC-H) were collected. Flow cytometry data were analysed using FlowJo software (http://flowjo.com).

2.4 | HPLC Analysis

HPLC was used to measure concentrations of aromatic compounds. All samples were centrifuged and filtered using a 0.2 μm cellulose nitrate syringe filter and mixed with an equal volume of methanol before being injected (1 mL/min gradient elution) into an Agilent 1260 Infinity II HPLC unit (Agilent Technologies, USA) fitted with an InfinityLab Poroshell 120 EC-C18 (4.6 × 150 mm) column and precolumn (4.6 × 5 mm). Solvents A (formic acid 0.1% in water) and B (formic acid 0.1% in methanol) were used as eluents, and the operating protocol was as follows: 20 μL injection volume, 4 min equilibration (solvent A 50%: solvent B 50%) between injections, solvent B applied at a 50% to 95% linear gradient for 10 min followed by 95% solvent B for 2 min. Column temperature was set to 35°C with detection wavelengths of 230 nm for *m*-toluate, 210 nm for benzyl alcohol and 270 nm for benzoate. Said protocol was also used with standards at known concentrations to plot calibration curves for subsequent quantification of compound concentrations.

2.5 | Adaptive Laboratory Evolution Experiments

For adaptive laboratory evolution 1 (ALE1), a single colony of the strain SBG1390 was selected from solid LB medium, inoculated into 10 mL LB medium, and incubated overnight at 30°C, agitated at 170 rpm. Then, the culture was transferred (final OD_{600} of 0.15) to a 100 mL Erlenmeyer flask double sealed with parafilm containing 20 mL of M9 minimal medium supplemented with 5 mM glucose plus 4 mM toluene. The flask culture was incubated at 30 °C, agitated at 170 rpm. After the culture reached the stationary phase, optical density was measured to record the number of generations, calculated using the formula: number of generations = $\ln(OD_{final}/OD_{initial})/\ln(2)$ (Bentley et al. 2020) and cells were transferred to fresh medium. This serial passage process was conducted 5 times (11.6 generations approximately) when the concentration of toluene was increased up to 6 mM. At approximately generation 28.5, glucose was removed from the media.

For adaptive laboratory evolution 2 (ALE2), a single colony of the strain SBG1071 was selected from solid M9 minimal medium supplemented with 5 mM *m*-toluate. The colony was transferred to a 100 mL Erlenmeyer flask double sealed with parafilm containing 20 mL of M9 minimal medium supplemented with 2 mM *m*-xylene. The flask culture was incubated at 30°C, agitated at 170 rpm. After the culture reached the stationary phase, the optical density was measured and cells were transferred (final OD_{600} of 0.15) to fresh medium. After this first passage,

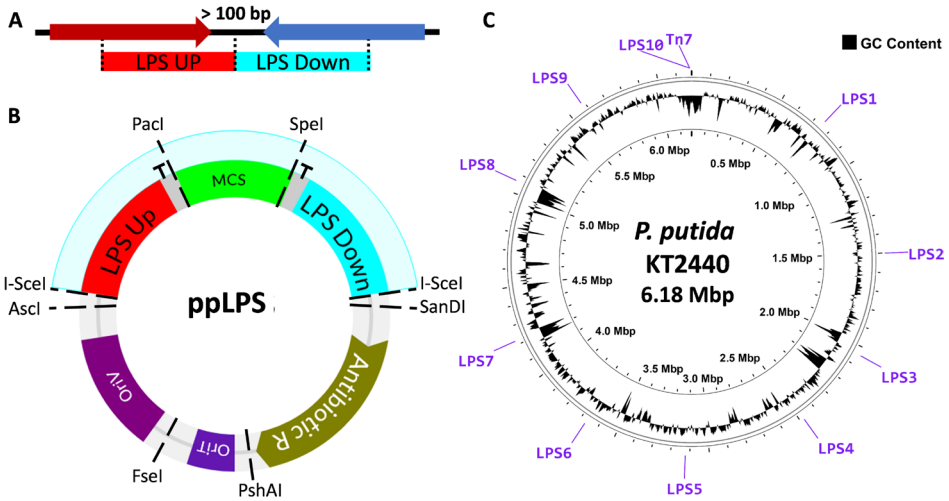

FIGURE 1 | Overview of ppLPS structure and integration locus. (A) Schematic representation of LPS regions. (B) ppLPS vectors contain an integrative region comprising LPS Up (red), a multicloning site (MCS) (green), LPS Down (light blue) and two strong bidirectional transcriptional terminators flanking MSC (grey). (C) Map of *P. putida* KT2440 genome indicating the position of LPS loci and the *att*Tn7 position. GC content illustrates the GC-Profile of *P. putida*.

the concentration of *m*-xylene was increased up to 4 mM. At generation 3.6, *m*-xylene was increased up to 6 mM.

2.6 | Competition Assay

SBG1084::YFP, MT2::RFP, SBG1084::RFP and MT2::YFP strains were grown overnight (30°C) in M9 minimal medium supplemented with 0.2% glucose and 1 mM toluene. Culture strains fitted with YFP-RFP (and vice versa) were diluted and mixed in M9 minimal medium with toluene 6 mM as the only carbon source. Single-cell flow cytometry was used to measure the composition of the population at T = 0 h and after 20 h (once cultures had reached the stationary phase). At this point, cultures were diluted in fresh M9 medium with toluene.

2.7 | Genome Sequencing

Whole-genome sequencing of the *P. putida* KT2440 and SBG1084 strains was conducted at MicrobesNG, University of Birmingham, Birmingham, UK. Libraries were built using the Nextera XT kit (Illumina, San Diego, CA, USA) and sequenced on the Illumina HiSeq platform (Illumina).

Circular diagrams of bacterial genome sequences with locus integration and GC content were generated using the Proksee online tool (Grant et al. 2023).

3 | Results

3.1 | Identification of LPS Integration Sites and ppLPS Vector Architecture Design

Assuming that the expression of genes in bacterial genomes is influenced by their distance to the origin of replication (Block et al. 2012), we made a conscious decision to choose specific locations across the chromosome of *P. putida* KT2440 as potential LPS. We first focused on intergenic regions longer than 100 bp between convergent genes. This selection criterion aimed to prevent interference with gene expression while maintaining the functionality of adjacent genetic elements, thereby avoiding polar effects on neighbouring genes. Overall, we analysed over 150 regions, identifying unique sequences to prevent unspecific homologous recombination events. Regions with sRNA transcripts were discarded to prevent potential post-transcriptional gene regulation events (Bojanovič et al. 2017). Likewise, prophage regions (Martínez-García et al. 2015) were discarded to avoid spontaneous excision events (Quesada et al. 2012). From the 17 LPS that met these criteria, we selected 10 LPS evenly distributed across the chromosome of *P. putida* KT2440 (Figure 1C, Table S4).

Each LPS comprises an upstream region and a downstream region, each containing half of the intergenic region along with fragments of the adjacent genes (Figure 1A). LPS design was set to 600 bp in length to facilitate homologous recombination and chromosomal integration. LPS assembly followed the SEVA architecture (Martínez-García et al. 2023), thus rendering ppLPS vectors SEVA siblings (Figure 1B). Specifically, the ppLPS vector structure comprises (i) an R6K origin of replication sandwiched by AscI-FseI restriction enzyme sites, (ii) a gentamycin gene for antibiotic resistance between SanD-PshAI restriction enzyme sites, and (iii) a multicloning site (MCS) between PacI-SpeI restriction enzyme sites to facilitate cloning of exogenous DNA. To prevent unwanted transcriptional interference with neighbouring genes, we positioned strong bidirectional transcriptional terminators (L3S3P41 and ECK120010858-R [Chen et al. 2013]) flanking the MCS. This arrangement ensured that an isolated environment was provided for the heterologous DNA. ppLPS vectors harbouring the R6K origin of replication are suicide plasmids for bacteria lacking the *pir* gene-encoded π protein. Such is the case with *P. putida*. Consequently, upon antibiotic selection, these vectors integrate into the chromosome at the designated LPS region (LPS Up or Down) through homologous recombination (Figure S1). Finally, the I-SceI recognition sites flanking

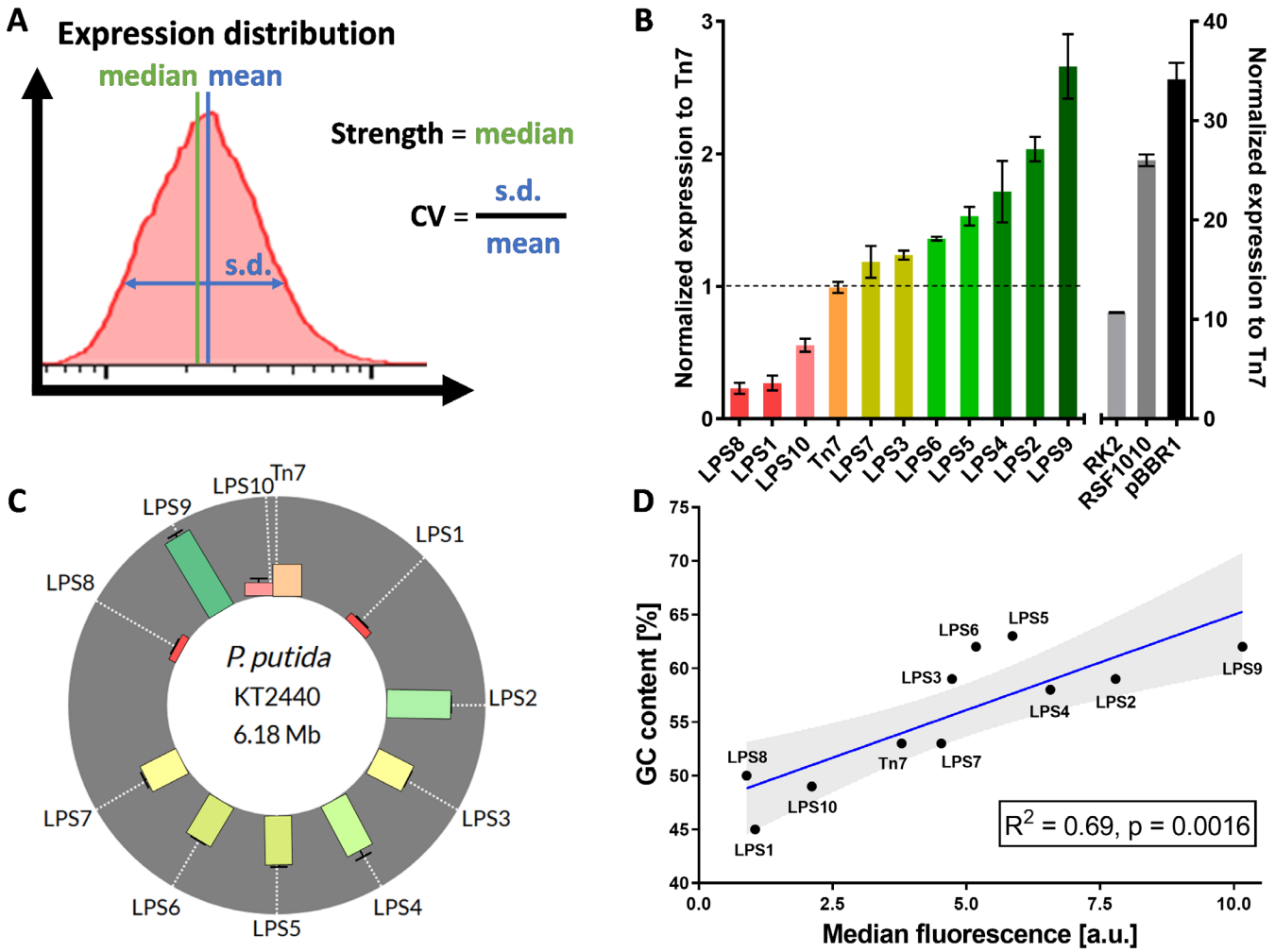

FIGURE 2 | Expression performance at different loci and plasmids. (A) Expression distributions are characterised by their median and noise (normalised standard deviation, i.e., coefficient of variation). (B) Normalised expression of pem7GFP construction to Tn7 at different LPS positions (monocopy) and with plasmids harbouring RK2, RSF1010 and pBBR1 origin of replications (multicopy). The error bars show the standard deviation of at least 2 independent biological replicates. (C) Effect of chromosomal location on gene expression. (D) Correlation between the GC content (%) of 2 kb fragments surrounding the integration position and the intensity of GFP fluorescence expressed at different positions.

LPS regions support targeted editing of the bacterial genome (Martínez-García and de Lorenzo 2011). Initially, the collection of ppLPS vectors was designed for gentamicin resistance. However, it is possible to replace the antibiotic resistance cassette with others available on the SEVA platform depending on specific experimental requirements.

3.2 | Leveraging *P. putida*'s Chromosome for Variable Gene Expression Control

The ppLPS system consists of a collection of 10 vectors (ppLPS1 to ppLPS10) tailored to target specific loci along the *P. putida* chromosome (Figure 1C). To assess gene expression strength in the ppLPS library, the GFP reporter gene was first cloned in all 10 LPSs under the control of the pem7 constitutive promoter. The resulting plasmids were used to integrate the reporter TU in the corresponding genome locations. As a control, this same construct was introduced into the *Pseudomonas* chromosome using the Tn7 system (Zobel et al. 2015) (Table S1). Finally, the fluorescence intensity of the recombinant strains was measured using flow cytometry during mid-exponential phase in M9 minimal medium supplemented with 20 mM glucose (Figure 2A). Interestingly, we observed a wide range of expression profiles depending on the specific LPS used for integration. Comparing expression levels against the *att*Tn7 reference, we identified three distinct groups (Figure 2B). The first group consisted of LPS positions with lower expression strength than *att*Tn7, that is, LPS8, LPS1 and LPS10. The second group included LPS positions displaying expression strengths similar to the reference, that is, LPS7, LPS3, LPS6 and LPS5. The third group comprised LPS positions with more than double the expression strength of attTn7, that is, LPS4, LPS2 and LPS9. Interestingly, the strains harbouring this group of LPSs exhibited a reduced growth rate, likely due to the greater metabolic burden resulting from GFP expression, as previously reported (Zobel et al. 2015).

To thoroughly characterise the ppLPS library, we further assessed the levels of expression noise associated with each individual position in the genome. Noise correlates with fluctuations in gene expression caused by factors other than distance to the origin of replication (oriC), such as DNA topology

and/or promoter architecture. We subsequently measured the difference in gene expression between cells to define a coefficient of variation (CV). Interestingly, regardless of their position in the chromosome and their expression strength, all LPSs displayed similar noise levels and no substantial differences were found in CV values (Figure S2). Altogether, our data showed that the ppLPS vector collection exhibited a broad range of gene expression levels with negligible differences in expression noise.

3.3 | ppLPS Expression Strength Is Determined Primarily by Genome Context Rather Than Distance to ORI

Previous studies have shown that gene expression levels can vary depending on genomic location. Specifically, positions closer to the *oriC* can result in high levels of expression, as observed in *Bacillus subtilis* (Sauer et al. 2016) and *E. coli* (Goormans et al. 2020). However, we did not record such behaviour using our ppLPS device. Instead, our findings indicated significantly lower levels of expression for several LPS positions close to the oriC, including LPS1, LPS8 and LPS10 (Figure 2C). This apparent discrepancy could be attributed to the genomic context of each LPS and/or to recently highlighted physical constraints imposed by DNA bending (Shen and Landick 2019). We studied this in further detail and found an interesting correlation between the GC content in the vicinity of each LPS and GFP expression. Specifically, a higher GC content was associated with a greater degree of gene expression ($R^2 = 0.69$, $p = 0.0016$) (Figure 2D). Therefore, LPSs with the lowest GC content (LPS1 45%, LPS8 50% and LPS10 52%) also exhibited the lowest expression levels. On the contrary, LPSs with moderate/high GC contents such as LPS9, LPS2 and LPS5 consistently showed high levels of gene expression irrespective of their position in the genome (Figure 2D). Interestingly, LPS9, which has a high GC content (62%) and is located near the oriC, exhibited the highest reporter activity. In contrast, position *att*Tn7, with a lower GC content (53%) and commonly used as a reference for gene integration in *P. putida*, showed lower expression levels compared to most of the LPS positions in this study, despite also being near the oriC.

3.4 | Contextualising the Expression Profile of the ppLPS System

It is widely accepted that multiple copies of plasmidic TUs typically yield higher levels of expression than if they were to be integrated as single copies into the chromosome. However, a thorough and standardised comparison of gene expression levels between these systems has surprisingly garnered limited attention, therefore leading to the existence of a notable gap in quantitative measurements within this area of research. To address this knowledge gap in *P. putida*, we conducted a study to quantify the expression profiles of a reference TU present in a collection of plasmids featuring different ORIs and copy numbers (pBBR1, RK2 and RSF1010). We subcloned the pem7GFP TU from ppLPS vectors into plasmids pSEVA221 (RK2 origin), pSEVA231 (pBBR1 origin) and pSEVA251 (RSF1010 origin). Fluorescence of the resulting strains was measured using flow cytometry under the same conditions as before and compared with the *att*Tn7 position. As could be expected, we found that fluorescence correlated with the expected copy number, with plasmid pSEVA221-pem7GFP (RK2 origin) registering the lowest levels of fluorescence. Nevertheless, even this RK2-based plasmid showed an expression level 10.6-fold higher than the reference *att*Tn7 position. Notably, this plasmid's expression was in the same order as the strongest LPS (only 3.9-fold greater than the LPS9 position) (Figure 2B). Plasmids with RSF1010 and pBBR1 origins exhibited similar expression profiles, with fold expression values of 26.3 and 34.4 respectively when compared to *att*Tn7. In resemblance to our findings for LPSs, no substantial expression noise was observed for these plasmid systems. However, the plasmid RK2 presented a slightly higher CV, likely due to this plasmid having the lowest copy number, likely promoting greater heterogeneity in gene dosage. In summary, using the expression of the attTn7 position as a benchmark, we demonstrated that the expression strength for a heterologous TU in KT2440 can be fine-tuned to return 0.2–2.7-fold increases using the ppLPS system. Furthermore, this range can be significantly bolstered to 10.6–34.4-fold increases using replicative plasmids.

3.5 | Rational and Spatial Redesign of the Metabolism of Aromatic Hydrocarbons in *P. putida* KT2440

Significant phenotype engineering requires the incorporation of multiple metabolic pathways/operons and their subsequent optimization in terms of expression and performance. However, challenges arise when multiple pathways/operons require iterative integrations. Hence, we undertook the challenging task of validating our GENIO approach by (re)introducing a complex phenotype in *P. putida* KT2440, namely the ability to utilise aromatic hydrocarbons as the sole carbon and energy source. It is worth noting that the KT2440 strain is a derivative of the toluene and *m*-xylene degrader *P. putida* mt-2 strain, and that this phenotype was lost during isolation (Regenhardt et al. 2002). The degradation of toluene and *m*-xylene by mt-2 is facilitated by three clusters present in the pWW0 (TOL) plasmid (Figure 3A). These gene clusters comprise an 8.5 kb Upper operon (*xylUWCMABN*) which is responsible for the conversion of toluene/*m*-xylene to benzoate/*m*-toluate, an 11.5 kb Meta operon (*xylXYZLTEGFJQKIH*) involved in the subsequent conversion of these compounds into TCA intermediates via catechol/3-methylcatechol, and a 3.1 kb regulatory node (*xylR-xylS*) supporting proper expression of the Upper and Meta operons. Therefore, the selection of this complex pathway for integration into the chromosome of *P. putida* serves as proper proof of concept to effectively validate the performance of our new method.

We tested GENIO by optimally (re)constructing the toluene/*m*-xylene pathway in *P. putida* KT2440. Specifically, we delivered a fully performing (re)construction of the toluene/*m*-xylene pathway in two iterative phases. First, we constructed a synthetic hybrid pathway for toluene catabolism using the Upper operon and the native Ortho pathway for benzoate catabolism present in *P. putida* (Figure 3A). The second phase focused on the inclusion of the Meta operon to expand the metabolic versatility of *P. putida* towards methyl benzoate, and thus *m*-xylene.

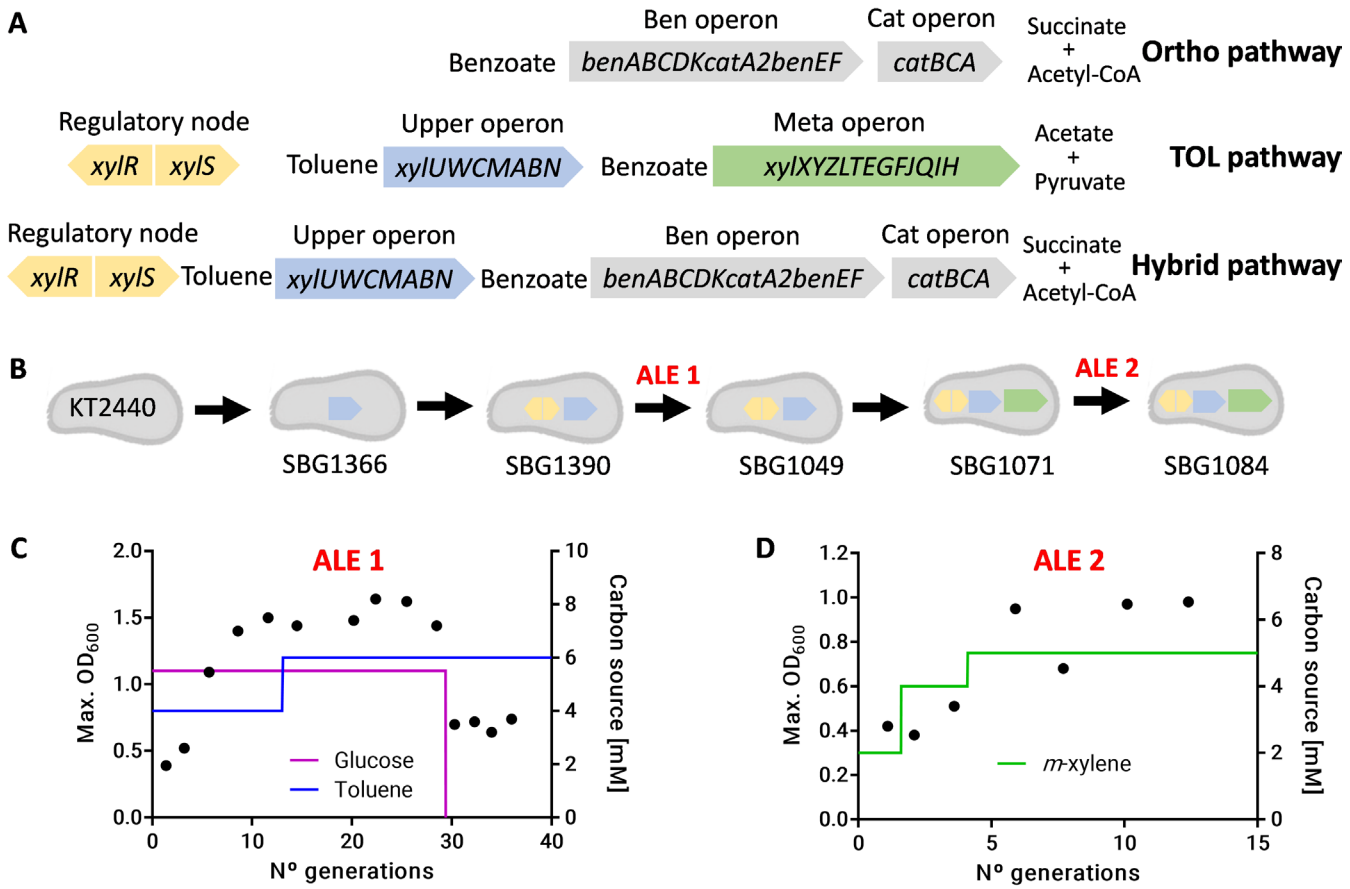

FIGURE 3 | (A) Schematic representation of the TOL pathway for toluene catabolism encoded in the TOL plasmid, *P. putida*'s Ortho pathway for benzoate catabolism and the hybrid pathway. (B) Engineered strains construction workflow. The Upper operon is marked blue, the regulatory node is marked yellow and the Meta operon is marked green. (C) Adaptive laboratory evolution (ALE 1) experiment with strain SBG1390 using glucose and toluene as carbon sources. (D) Adaptive laboratory evolution (ALE 2) experiment with strain SBG1071 using *m*-xylene as carbon source. Optical density was measured after 24 h of incubation.

3.5.1 | Engineering a Synthetic Hybrid Pathway for Toluene Catabolism in *P. putida*

Considering that the catabolism of catechols is a well-known bottleneck in the degradation of aromatic compounds (George and Hay 2012, 2011; Jiménez et al. 2014; Muñoz et al. 2007), we strategically integrated the Upper operon into the LPS6 site. This particular genomic location provides a moderate level of expression; therefore, preventing excess accumulation of catechol in the engineered strains (Figure 3B). To ensure optimal dosage of regulatory elements without inducing any detrimental effects on the cell, we then integrated regulatory node *xylR-xylS* into the high and low expression sites LPS9 (high) and LPS8 (low). Notably, successful integrations of the regulator operon occurred exclusively at the LPS8 position (strain SBG1390, Figure 3B). This suggests that high-rate expression of *xyl* regulators may have a negative effect on the cells, as occurs with other regulators due to their intrinsic insolubility and their tendency to form inclusion bodies. This result greatly enhances the value of the ppLPS platform by supporting a wide range of expression rates to deliver accurate control over the expression of potentially toxic genes.

The engineered hybrid pathway involves toluene metabolism to benzoate through the Upper pathway and subsequent metabolism of benzoate via the *ben*, *cat* and *pca* genes from the Ortho pathway encoded in the chromosome of *P. putida* (Jimenez et al. 2002). The theoretical model supports that SGB1390 grows on toluene as the sole carbon source. However, strain SBG1390 was unable to grow directly on toluene at 6 mM. This could be partly attributed to the fact that *P. putida* KT2440 lacks the inherent capability to metabolise toluene and, instead, perceives this hydrocarbon as a stressor rather than as a nutrient despite the presence of the Upper operon (Domínguez-Cuevas et al. 2006). However, the possibility that suboptimal expression of the Upper operon and/or the potential toxicity of intermediate metabolites might have hindered growth could not be dismissed. Hence, we decided to use adaptive evolution as a potentially viable solution to tackle a scenario where the initial integration of heterologous operons in the genome yielded suboptimal outcomes (Agozzino et al. 2020). We set up an adaptive evolutionary experiment to culture multiple generations of strain SBG1930 in the presence of glucose while gradually increasing the concentration of toluene (ALE 1, Figure 3C). After 30 generations, cells acquired the ability to grow efficiently on toluene (6 mM) as the sole carbon and energy source. We isolated and phenotyped 10 individual cells from this adapted culture and singled out the strain showing the most promising performance in terms of biomass production from toluene (strain SBG1049) for further study (Figure 3B and Figure S3).

3.5.2 | Reconstruction of the *m*-Xylene Pathway in *P. putida* KT2440

The Meta operon is required to degrade *m*-xylene because the native Ortho pathway cannot catabolise *m*-toluate. We thus cloned the Meta operon in the mid and high expression level plasmids ppLPS5 (medium) and ppLPS9 (high). Subsequently, these plasmids were integrated into the chromosome of strain SBG1049. In order to trigger the second recombination event to obtain recombinant strains, cells were plated on M9 minimal medium with *m*-toluate at a concentration of 5 mM (*m*-toluate serves as both an inducer for the I-SceI system and a carbon source for cells harbouring the Meta operon). Colonies were observed only when the Meta operon was integrated at the LPS9 position, which corresponds to the position with the highest expression level, that is, almost twice that of the LPS5 position (Figure 1B). A high flux through the Meta pathway is essential to avoid the accumulation of *m*-toluate and its further transformation to 2-methyl-2-enelactone, a non-degradable and lethal compound for *P. putida* (de Lorenzo and Joshi 2019). On the whole, our data suggest that the expression of the Meta pathway at the LPS5 position results in a suboptimal flux that is incompatible with cell survival. This called for LPS9's potential ability to deliver a greater flux.

The resulting strain (*P. putida* SBG1071), which harbours the regulatory node and the Upper and Meta operons, was able to grow directly on *m*-xylene as the sole carbon source. These experiments highlighted the importance of adequately balancing the levels of expression of the operons responsible for a complex phenotype. We then moved on to a second adaptive evolutionary experiment designed to further optimise *m*-xylene metabolism in *P. putida* (ALE2, Figure 3D). This resulted in the final strain SBG1084, which improved biomass production at the expense of a high concentration of *m*-xylene (Figure 3D).

3.6 | GENIO Enables Optimal Hydrocarbon Catabolism in *P. putida* KT2440

P. putida mt-2 is fitted with an efficient *m*-xylene and toluene metabolism optimised through extensive cultivation on said compounds as sole carbon and energy sources (Worsey and Williams 1975). Consequently, comparing the growth performance of strains mt-2 and SBG1084 on aromatic hydrocarbons should not only return valuable insights into their growth and metabolic abilities, but also serve as an ideal approach to contextualise the GENIO workflow.

When toluene was used as a carbon source, strain SBG1084 exhibited a shorter lag phase compared to strain mt-2 (Figure 4A). This suggests that strain SBG1084 has a more efficient and rapid response to toluene as a carbon source. Additionally, strain SBG1084 displayed a slightly lower accumulation of intermediates with faster depletion of benzyl alcohol and negligible benzoate secretion (Figure 4A). This finding supports the notion of an increased metabolic flux through the Meta/Ortho pathways in the engineered strain. When *m*-xylene was used as the carbon source, both strains exhibited a similar phenotype, including identical duration of the lag phase and parallel accumulation of *m*-toluate in the medium (Figure 4B). This could indicate that the growth performance and metabolic capabilities of the two strains had similarities in this nutritional scenario.

To assess the relative fitness and competitive advantage of the engineered SBG1084 strain over the native mt-2 strain, if any, we conducted a series of competition experiments using toluene as a carbon source. Both strains were labelled with specific reporter proteins to enable accurate tracking and differentiation within the mixed population. To rule out potential biases caused by the metabolic burden attached to protein expression, we cross-labelled the strains with RFP and GFP (Figure 4C). Finally, mixed cultures starting with equal proportions of both strains (~50% of each) were grown on toluene, and we used flow cytometry to monitor the population's growth dynamics. These competition experiments showed that strain SBG1084 had a significant growth advantage over strain mt-2. SBG1084 was able to rapidly adapt and utilise toluene as a carbon source more efficiently. Over several generations, an increase in the proportion of SBG1084 could be observed in the mixed population. Eventually, despite reaching an equilibrium state where the two strains coexisted, SBG1084 accounted for over 90% of the population's total cells irrespective of the reporter protein used (Figure 4C).

3.7 | Optimal Aromatic Hydrocarbon Metabolism Is Supported by a Large Chromosomal Rearrangement in Strain SBG1084

To gain deeper insight into the genotype–phenotype relationship of strain SBG1084, we sequenced its genome and analysed it in depth to identify any potential changes or alterations in the chromosome arising from the evolutionary process. Interestingly, this analysis revealed an important chromosome rearrangement that was likely responsible for the evolved strain's efficient toluene and xylene metabolism. Specifically, we found a deletion event spanning 46,326 bp in close proximity to a region with a high number of sequencing reads (Figure 5A, Table S5). Upon closer analysis, we established that this region was a large genomic duplication of 422,448 bp spanning positions 3,316,840 to 3,730,589 (Figure 6A, Table S6). The fragment was not only duplicated but also inverted, and it took up the vacant space left by the deletion (Figure 5A). The identical fragments were separated by a region of 5449 bp.

The mechanisms underlying gene duplication can vary depending on their specific genomic context (Reams and Roth 2015). In this case, we could not determine the relevant recombination mechanism. However, one of the borders of the duplicated region encoded several transposases and integrases, as well as a phage recombinase at islands 56 and 57 (Weinel et al. 2002). Functional analysis of the duplicated fragment encoding 432 genes revealed a wide range of COG functions (Figure S4A). Notably, duplicated functions included several aromatic pathways, including part of the toluene hybrid pathway (toluene Upper operon and ben genes), phenylacetic acid and trinitrotoluene. Cytosine, putrescine/spermidine and hydroxybutanoate pathways, among others, were also present.

Regarding functional losses as a result of the deletion event affecting the region between 3,736,040 and 3,782,365, we identified up to 46 locus tags, a significant portion of which were associated with COGs related to inorganic transport and metabolism (Figure S4B). Given that many of these transporters lack

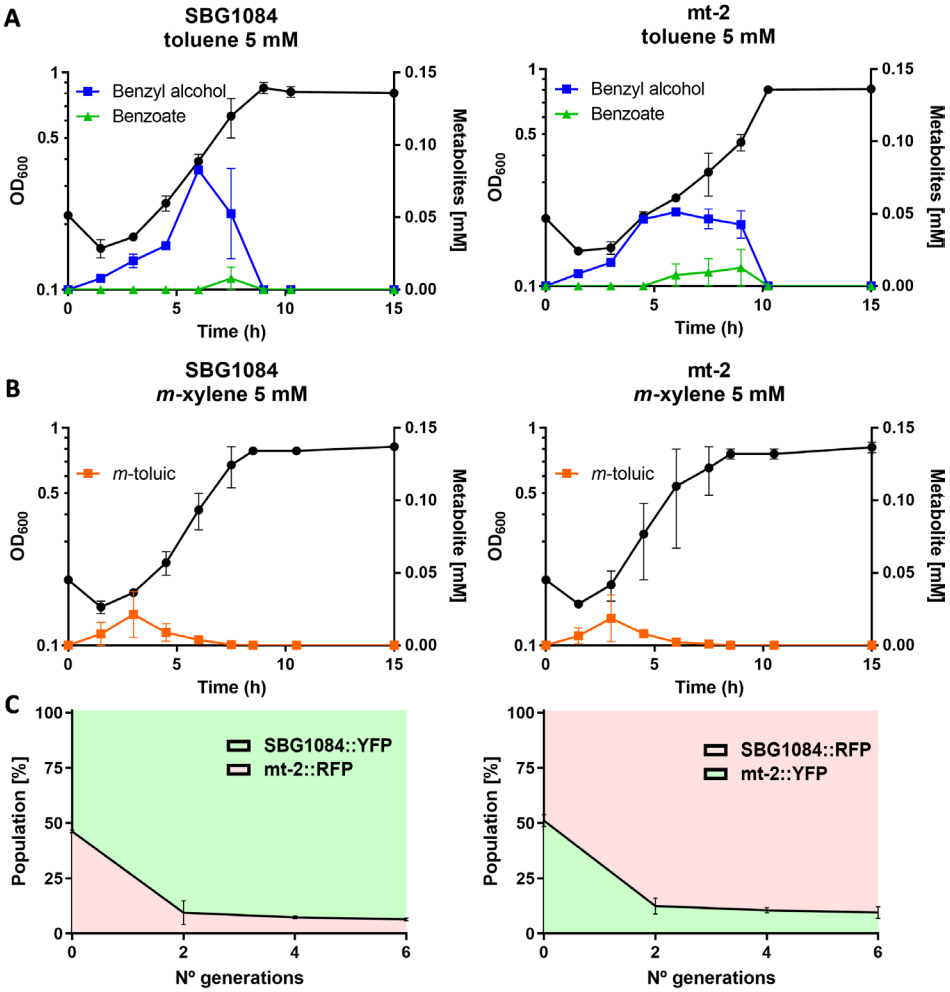

FIGURE 4 | Growth performance of strains SBG1084 and mt-2. (A) Growth curves of strains SBG1084 and mt-2 on toluene (5 mM) as the sole carbon source. Accumulation of metabolites in the culture was measured by HPLC at the times indicated. (B) Growth curves of strains SBG1084 and mt-2 on *m*-xylene (5 mM) as the sole carbon source. (C) Relative abundance of SBG1084 and mt-2 cells in a mixed population growing on toluene 5 mM as the sole carbon source. Population distribution was determined by flow cytometry. Aggregated cells registering both fluorescence signals were ~1.1% ± 0.6%, while dead cells were 2.4% ± 0.8% (data not shown). Results show the average values of data collected from two independent experiments.

known functions, further identification of specific functions was challenging. However, we did observe an operon likely encoding an ABC transport system for nickel located on genomic island 66.

Finally, we found an interesting single nucleotide insertion in the Upper operon's gene *xylN* which encodes for the outer membrane's xylene porin. This mutation introduces an additional cytosine, leading to a frameshift mutation that introduces premature stop codons and renders the resulting porins non-functional. Similar mutations have been associated with increased resistance to *m*-xylene by reducing the permeability of the aromatic compound across the outer membrane (Kasai et al. 2001).

To trace the evolutionary trajectory of strain SBG1084 (Figure 5B) we analysed the intermediate strains using PCR to correlate genomic changes with specific evolutionary scenarios. Interestingly, we found that the large chromosomal rearrangement was present in SBG1049 but not in SBG1390, indicating that it occurred during the ALE 1 experiment (where toluene was the sole carbon source). This is consistent with the duplication of part of the hybrid toluene pathway promoting efficient toluene metabolism. Whether the remaining duplicated and/or deleted genes contribute to the improvement of toluene metabolism or they are a consequence of the mechanisms driving duplication remains unknown and challenging to address.

On the other hand, the mutation affecting *xylN* was only found in SBG1084. This indicates that it appeared during the ALE 2 experiment, where xylene was the carbon source, since a truncated XylN likely contributes to limiting the entry of xylene into the cell, avoiding toxicity.

3.8 | The Acquisition of Aromatic Hydrocarbon Metabolism Has a Negligible Impact on Fitness in Alternative Growth Scenarios

Alongside the advancement of evolutionary engineering in bacteria, there is a growing acceptance that the fitness gain in response to evolutionary pressure may lead to reduced

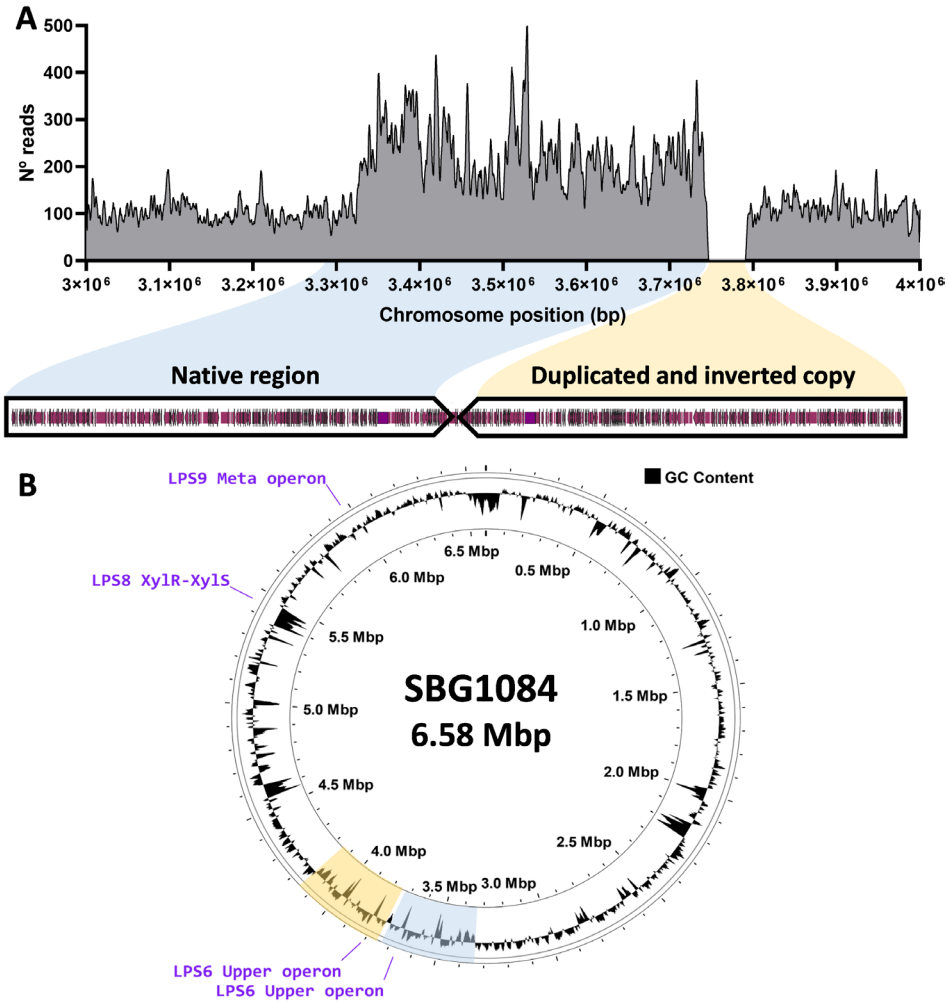

FIGURE 5 | (A) Read coverage of SBG1084's genome sequencing from chromosome position 3–4 Mb. A duplicated region is shaded in light blue with 3-fold higher sequencing coverage. The gap represents a deleted region with no reads replaced with the duplicated fragment (shaded in light orange). (B) Genome map of strain SBG1084 displaying GC content. The duplicated native region is shaded in light blue and the duplicated/inverted region is shaded in light orange.

fitness in alternative nutritional conditions (Jerison et al. 2020). Nevertheless, the impact on fitness ultimately depends on the balance between the benefits and costs associated with the optimisation of the new metabolic trait. Therefore, we set out to understand the impact of strain SBG1084's genetic rearrangement by growing it in selected environmental scenarios and comparing its performance to that of its parental strain *P. putida* KT2440 (Figure 6). Remarkably, we observed no significant differences in fitness when utilising conventional carbon sources not affected by genome changes, such as glucose, succinate, citrate and 4-hydroxybenzoate (Figure 6A–D). This indicates that the chromosomal rearrangement resulted in a neutral outcome despite the increased metabolic burden caused by genome expansion (≈8%). We then became interested in evaluating potential positive effects on fitness due to increasing gene dosage. To investigate this, we tested the performance of strain SBG1084 on phenylacetate and 3-hydroxybutyrate, compounds whose catabolic pathways were either totally or partially duplicated. Similarly, we found negligible effects on fitness as a result of pathway duplication (Figure 6E,F). This suggests that the native configuration may already deliver optimal performance, thus rendering gene duplication for increased enzyme production unnecessary. However, the higher metabolic load that ensued from pathway duplication coupled with overexpression did not seem to have a negative effect. Altogether, our results strongly suggest that *P. putida* exhibits high robustness against increased metabolic burden as a result of genome expansion and/or overexpression.

One of the intermediates in the degradation pathway of toluene is benzoate, which KT2440 metabolises with its *ben* cluster. Despite having a duplicate *ben* cluster, SBG1084 did not show improved growth performance on benzoate. Instead, it registered impaired growth compared to KT2440 (Figure 6G). This apparent contradiction could be broadly explained by the fact that duplication of the *ben* cluster is not followed by duplication of the *cat* cluster responsible for catechol degradation, potentially leading to the accumulation of toxic levels of catechol inside the cell (Jiménez et al. 2014). On the other hand, strain mt-2, which metabolises benzoate through the *ben* cluster present in its genome and the Meta operon contained in the TOL plasmid, also showed impaired growth on benzoate, although to a lesser extent than SBG1084, which harbours two copies of the *ben* cluster and the Meta operon in the chromosome (Figure 6G).

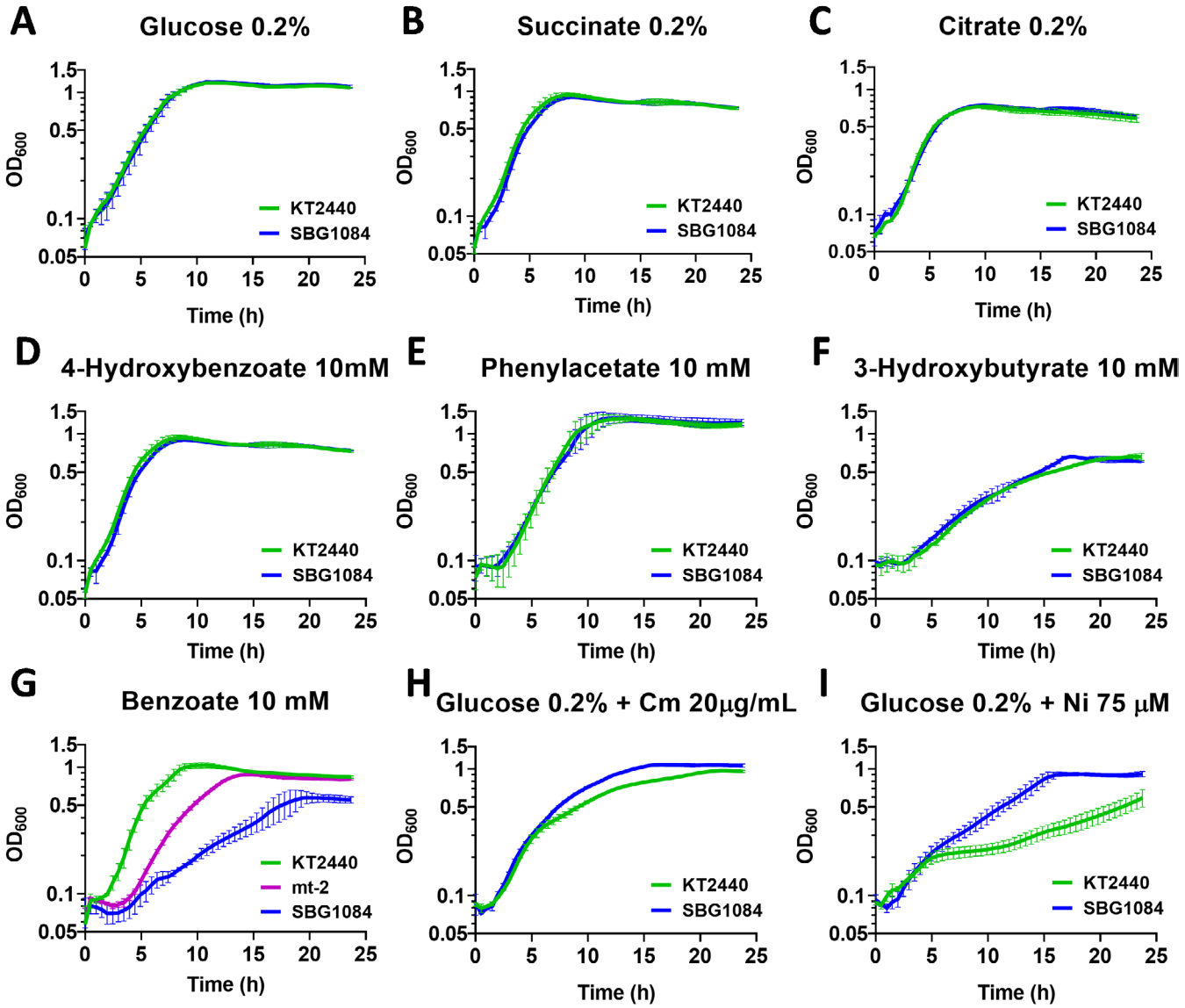

FIGURE 6 | Growth performance of *P. putida* KT2440, SGB1084 and mt-2. Logarithmic representation of cells grown in minimal medium M9 supplemented with glucose 0.2%, succinate 0.2%, citrate 0.2%, 4-hydroxybenzoate 10 mM, phenylacetate 10 mM, 3-hydroxybutyrate 10 mM, benzoate 10 mM, glucose 0.2% amended with chloramphenicol 20 μg/mL, or glucose 0.2% amended with nickel 75 μM. Growth curves are the average of at least two independent experiments.

Cardiolipin biosynthesis genes (PP_3263–3266) were also present in the duplicated region. Cardiolipin is an important component of the bacterial membrane and plays a role in different stress responses (Bojanovič et al. 2017). Previous research showed that a *P. putida* cardiolipin synthase mutant exhibited increased sensitivity compared to the wild-type strain when exposed to toluene or chloramphenicol (Bernal et al. 2007). We implemented growth experiments using glucose as a carbon source supplemented with chloramphenicol at 20 μg/mL to assess the potential impact of the duplicated cardiolipin biosynthesis genes in SBG1084 (Figure 6H). SBG1084 performed better than KT2440 in the presence of chloramphenicol, suggesting that increased levels of cardiolipin may contribute to stress resistance. Additionally, SBG1084's enhanced performance on toluene (Figure 4A) could also be supported by the duplication of cardiolipin synthesis genes.

Finally, we investigated the impact on fitness caused by the deletion event. Considering that it was the only gene cluster with a well-known function, we focused on PP_3341–3344, which is involved in nickel transport. Since nickel is an obligate micronutrient but is toxic at high concentrations (Ray et al. 2012), we used growth on glucose amended with 75 μM nickel as a proxy to assess the effect of the deletion (Figure 6I). SBG1084 performed better than KT2440, which suggests that deleting the nickel ABC transporter provides the cell with extra protection against nickel toxicity by preventing its entry into the cytoplasm.

4 | Discussion

The ppLPS system enabled rapid and marker-free integration of genetic constructs, making it an efficient genome expansion

tool for *P. putida* KT2440. With 10 well-characterised integration sites, ppLPS additionally offers an extra layer of transcriptional regulation control. This approach provides a means to explore the fitness landscape and identify optimal locations for gene expression. Moreover, we demonstrated that this rational genome integration system followed by evolutionary engineering (GENIO approach) supports the optimisation of genetic determinants and their contextualisation within the metabolic and genetic background of the host strain. Therefore, GENIO allows for multidimensional optimisation to fine-tune suboptimal configurations for optimal fitness. GENIO was fully validated by rationally (re)designing *P. putida*'s complex aromatic hydrocarbon metabolism, a process that involved (de)constructing the pathway and finely balancing the expression levels of its basic components. Overall, GENIO delivers a significant advancement in the field of synthetic biology with *P. putida*, offering researchers solid ground to explore genome integration and the fitness landscape. An additional significant outcome of our study is that, while previous studies only compared the loci expression patterns between themselves (Chaves et al. 2020) and/or Tn7 attachment site (Köbbing et al. 2024), we have compared and contextualised heterologous expression in terms of cis (at different locations in the chromosome) and trans configurations using several different plasmids and copy numbers (Figure 3B). Interestingly, the comparison of strength expression space between our system and Köbbing's library, which share the identical reference (Tn7 site), showed a broader expression range in GENIO (Figure S5), potentially offering a wider range of solutions.

4.1 | Expression of the ppLPS System Is Primarily Governed by Intrinsic Genome Constraints Rather Than Spatial Patterns

Among the multiple factors affecting gene expression, the physical location of a gene in the chromosome has been identified as a major contributor. Many reports have shown that both gene expression and gene dosage are increased near the origin (Block et al. 2012; Couturier and Rocha 2006; Lato and Golding 2020; Sauer et al. 2016). Moreover, a recent systematic study covering all protein-coding genes from *E. coli*, *B. subtilis* and *Streptomyces* identified a positive correlation between gene expression and distance to the ORI. Therefore, for most replicons, genes closer to the origin of replication exhibit higher expression levels (Lato and Golding 2020).

Despite being based on the degree of expression of selected genome locations instead of a systematic analysis, our results suggest that, at least for the ppLPS system, gene expression strength in the *P. putida* genome is primarily driven by factors other than spatial patterns. The expression profile observed in our study (Figure 2B) could instead be attributed to structural constraints such as DNA bending and/or nucleoid-associated proteins (Histone-like Nucleoid-Structuring proteins H-NS). These proteins play an important role in gene expression by transcriptionally repressing AT-rich regions in bacterial genomes (Dorman 2004; Navarre et al. 2007; Qin et al. 2019). In *P. putida*, with an average GC content of 61.6% (Weinel et al. 2002), TurA (H-NS-like MvaT class of transcription regulators) acts as a repressor for genes with atypically lower GC contents (Renzi et al. 2010). Therefore, TurA could be primarily responsible for downregulating the expression of LPS1, LPS8 and LPS10 irrespective of their proximity to the ORI. This regulatory mechanism may also explain the low expression levels observed for the mKate construct at the PP_5388 insertion locus, which has the lowest GC content (53%) among the tested positions (Chaves et al. 2020). Furthermore, recent research with *E. coli* has demonstrated a correlation between flanking GC content and modifications in canonical cis regulatory elements, thus supporting an influence of GC content on gene expression regulation (Scholz et al. 2022). Evidence suggests that the specific location of a gene within the genome, along with its surrounding genetic elements and regulatory sequences, has a more significant impact on its expression level than its distance to the origin of replication. This underscores the intricate relationship between genomic architecture and gene expression regulation.

4.2 | Engineering Complex Phenotypes Requires Synthetic Pathway Contextualisation Facilitated by Metabolic Robustness

Restoration of aromatic hydrocarbon metabolism in *P. putida* KT2440 has been a long-pursued goal in metabolic engineering. The very first attempts already revealed the potential of synthetic biology as it was beginning to emerge over 20 years ago. Ultimately, they resulted in the successful reconstruction of *P. putida*'s toluene and xylene metabolisms by reintroducing the Upper (Panke et al. 1998) and Meta (Williams et al. 1997) operons. These gene cassettes were extracted from the TOL plasmid and randomly integrated into the chromosome of *P. putida* using the Tn5 transposon, with strains selected based on their ability to grow on aromatic hydrocarbons. Although the resulting strains were not systematically analysed, neither genotypically nor phenotypically, these elegant studies demonstrated the feasibility of implanting complex phenotypes encoded by a large set of genes in *P. putida*. Here, we take over from pioneering authors to restore the toluene and *m*-xylene metabolism in KT2440 while systematically tracing the set of events required to deliver its optimal performance. Powered by GENIO, we have been successful in reaching far beyond a simplistic coupling of catabolic and regulatory genes.

While the ppLPS system enables spatial exploration for optimal performance, merely possessing the genetic blueprint proved insufficient. Additional genetic contextualisation of the synthetic pathway proved critical to ensuring cell survival (Figure 5A). Indeed, we documented a significant genome rearrangement in strain SBG1084 involving a large duplication (≈420 kb) and a more modest deletion (≈45 kb). Notably, the evolved strain exhibits enhanced competitiveness compared to its ancestral mt-2 strain when using toluene as a sole carbon source. This superior phenotype was likely driven, at least, by the duplication of the Upper operon and the native ben genes. Additionally, it seems reasonable to assume that the duplication of the cardiolipin biosynthesis pathway made SBG1084 more tolerant to toluene (Bernal et al. 2007; Ramos et al. 2015). Nevertheless, we cannot dismiss the possibility that some of the remaining duplicated and/or deleted genes may also contribute to this enhanced growth fitness.

Gene duplications, such as we observed in strain SBG1084, often arise due to positive selection. While the exact mechanism of

recombination driving this duplication and inversion event remains undefined (Moss et al. 2020), these duplications play a crucial role in the evolution of metabolic pathways, and they have been well documented in aromatic compound degradation (George and Hay 2011; van der Meer et al. 1992). Specifically, the amplification of particular alleles provides a selective advantage in certain environmental scenarios, even surpassing the cost of duplication itself (Maisnier-Patin and Roth 2015), as recently reported where a duplication in *P. putida* of 118,079 bp shows a positive effect on xylose utilisation (Dvořák et al. 2024). However, it is important to note that a genotype exhibiting high fitness under specific conditions may not sustain the same level of fitness outside of the selective environment. Indeed, studies have shown that the cost of carrying extra gene copies is substantial, with an estimated fitness reduction of 0.15% for each additional kilobase of DNA (Adler et al. 2014). Interestingly, our findings suggest a different scenario for *P. putida*. Firstly, the expansion of its genome by 424 kb did not impair fitness when using carbon sources unrelated to this rearrangement (e.g., glucose, succinate, citrate and 4-hydroxybenzoate). Secondly, duplicating or partially duplicating metabolic pathways not under selection, for example, phenylacetate and 3-hydroxybutyrate, resulted in neutral outcomes. This implies that the native configuration was likely already optimised, with minimal fitness costs due to extra gene dosage and overexpression. Our results strongly suggest that *P. putida* is highly robust against large genome expansions, thus enhancing its already excellent potential for biotechnological applications.

5 | Conclusion

GENIO facilitates ALE experiments in *P. putida*, and it additionally supports exploration of a more diverse genotypic space, thus reducing the likelihood of becoming trapped in local fitness maxima. By allowing researchers to choose from a variety of selected chromosomal locations, each associated with distinct local peaks of fitness, GENIO increases the odds of arriving at the desired phenotype. While GENIO may not provide an immediate solution to escaping local fitness peaks, it is a valuable tool to navigate the genotypic space until an optimal peak is found. Furthermore, we provide new insight into the intricate orchestration governing gene expression strength of the *P. putida* genome, strongly suggesting that it is primarily driven by intrinsic genome constraints rather than spatial patterns. Finally, GENIO has revealed *P. putida*'s high resilience against genome expansions, thus bolstering its biotechnological value.

Author Contributions

Blas Blázquez: investigation, writing – original draft, methodology, validation, visualization, formal analysis, data curation, conceptualization. **Juan Nogales:** conceptualization, funding acquisition, writing – original draft, writing – review and editing, project administration, supervision.

Acknowledgements

The authors would like to acknowledge Antonio Mesa for his assistance in the construction of some ppLPS plasmids and David San Leon and Francisco J. Canalejo for help provided with Figure 2. The help of Clive A. Dove in proofreading the manuscript is highly appreciated. We thank Prof. Victor de Lorenzo for providing us with the mt-2 strain, his critical review of the manuscript, and his valuable comments. This research received funding from the European Union's Horizon 2020 research and innovation programme under grant agreement numbers 814650 (SynBio4Flav), 870294 (MIX-UP) and 101000733 (PROMICON), as well as the TED2021-130689B-C33 (SyCoSys) and PID2022-139247OB-I00 (Rob3D) projects funded by MCIN/AEI/10.13039/501100011033 and European Union (Next Generation EU/PRTR) funding, a way to make Europe.

Conflicts of Interest

The authors declare no conflicts of interest.

Data Availability Statement

Data will be made available on request. Requests for materials should be addressed to the corresponding author. The ppLPS plasmids have been deposited at the SEVA database (https://seva-plasmids.com) and they are available upon request.

References

Abril, M. A., C. Michan, K. N. Timmis, and J. L. Ramos. 1989. "Regulator and Enzyme Specificities of the TOL Plasmid-Encoded Upper Pathway for Degradation of Aromatic Hydrocarbons and Expansion of the Substrate Range of the Pathway." *Journal of Bacteriology* 171: 6782–6790. https://doi.org/10.1128/JB.171.12.6782-6790.1989.

Acerenza, L. 2016. "Constraints, Trade-Offs and the Currency of Fitness." *Journal of Molecular Evolution* 82: 117–127. https://doi.org/10.1007/s00239-016-9730-3.

Adler, M., M. Anjum, O. G. Berg, D. I. Andersson, and L. Sandegren. 2014. "High Fitness Costs and Instability of Gene Duplications Reduce Rates of Evolution of New Genes by Duplication-Divergence Mechanisms." *Molecular Biology and Evolution* 31: 1526–1535. https://doi.org/10.1093/MOLBEV/MSU111.

Agozzino, L., G. Balázsi, J. Wang, and K. A. Dill. 2020. "How Do Cells Adapt? Stories Told in Landscapes." *Annual Review of Chemical and Biomolecular Engineering* 11: 155–182. https://doi.org/10.1146/annurev-chembioeng-011720-103410.

Andersson, D. I., and D. Hughes. 2010. "Antibiotic Resistance and Its Cost: Is It Possible to Reverse Resistance?" *Nature Reviews. Microbiology* 8: 260–271. https://doi.org/10.1038/NRMICRO2319.

Belda, E., R. G. A. van Heck, M. José Lopez-Sanchez, et al. 2016. "The Revisited Genome of *Pseudomonas putida* KT2440 Enlightens Its Value as a Robust Metabolic Chassis." *Environmental Microbiology* 18: 3403–3424. https://doi.org/10.1111/1462-2920.13230.

Bernal, P., J. Muñoz-Rojas, A. Hurtado, J. L. Ramos, and A. Segura. 2007. "A *Pseudomonas putida* Cardiolipin Synthesis Mutant Exhibits Increased Sensitivity to Drugs Related to Transport Functionality." *Environmental Microbiology* 9: 1135–1145. https://doi.org/10.1111/J.1462-2920.2006.01236.X.

Bentley, G. J., N. Narayanan, R. K. Jha, et al. 2020. "Engineering Glucose Metabolism for Enhanced Muconic Acid Production in *Pseudomonas putida* KT2440." *Metabolic Engineering* 59: 64–75.

Blázquez, B., D. San León, J. Torres-Bacete, et al. 2023. "Golden Standard: A Complete Standard, Portable, and Interoperative MoClo Tool for Model and Non-Model Proteobacteria." *Nucleic Acids Research* 51, no. 19: e98. https://doi.org/10.1093/NAR/GKAD758.

Block, D. H. S., R. Hussein, L. W. Liang, and H. N. Lim. 2012. "Regulatory Consequences of Gene Translocation in Bacteria." *Nucleic Acids Research* 40: 8979–8992. https://doi.org/10.1093/nar/gks694.

Bojanovič, K., I. D'Arrigo, and K. S. Long. 2017. "Global Transcriptional Responses to Osmotic, Oxidative, and Imipenem Stress Conditions in

Pseudomonas putida." *Applied and Environmental Microbiology* 83, no. 7: e03236-16. https://doi.org/10.1128/AEM.03236-16.

Chaves, J. E., R. Wilton, Y. Gao, et al. 2020. "Evaluation of Chromosomal Insertion Loci in the *Pseudomonas putida* KT2440 Genome for Predictable Biosystems Design." *Metabolic Engineering Communications* 11: e00139. https://doi.org/10.1016/j.mec.2020.e00139.

Chen, Y. J., P. Liu, A. A. K. Nielsen, et al. 2013. "Characterization of 582 Natural and Synthetic Terminators and Quantification of Their Design Constraints." *Nature Methods* 10: 659–664. https://doi.org/10.1038/nmeth.2515.

Cook, T. B., J. M. Rand, W. Nurani, D. K. Courtney, S. A. Liu, and B. F. Pfleger. 2018. "Genetic Tools for Reliable Gene Expression and Recombineering in *Pseudomonas putida*." *Journal of Industrial Microbiology & Biotechnology* 45, no. 7: 517–527. https://doi.org/10.1007/S10295-017-2001-5.

Couturier, E., and E. P. C. Rocha. 2006. "Replication-Associated Gene Dosage Effects Shape the Genomes of Fast-Growing Bacteria but Only for Transcription and Translation Genes." *Molecular Microbiology* 59: 1506–1518. https://doi.org/10.1111/j.1365-2958.2006.05046.x.

de Lorenzo, V., and H. Joshi. 2019. "Genomic Responses of *Pseudomonas putida* to Aromatic Hydrocarbons." In *Consequences of Microbial Interactions With Hydrocarbons, Oils, and Lipids: Biodegradation and Bioremediation*, 1–15. Springer Nature. https://doi.org/10.1007/978-3-319-44535-9_25-1.

Denamur, E., and I. Matic. 2006. "Evolution of Mutation Rates in Bacteria." *Molecular Microbiology* 60: 820–827. https://doi.org/10.1111/J.1365-2958.2006.05150.X.

Domínguez-Cuevas, P., J. E. González-Pastor, S. Marqués, J. L. Ramos, and V. de Lorenzo. 2006. "Transcriptional Tradeoff Between Metabolic and Stress-Response Programs in *Pseudomonas putida* KT2440 Cells Exposed to Toluene." *Journal of Biological Chemistry* 281: 11981–11991. https://doi.org/10.1074/jbc.M509848200.

Dorman, C. J. 2004. "H-NS: A Universal Regulator for a Dynamic Genome." *Nature Reviews. Microbiology* 2: 391–400. https://doi.org/10.1038/nrmicro883.

Dragosits, M., and D. Mattanovich. 2013. "Adaptive Laboratory Evolution – Principles and Applications for Biotechnology." *Microbial Cell Factories* 12, no. 1: 64.

Dvořák, P., B. Burýšková, B. Popelářová, et al. 2024. "Synthetically-Primed Adaptation of *Pseudomonas putida* to a Non-Native Substrate D-Xylose." *Nature Communications* 15, no. 1: 1–18. https://doi.org/10.1038/s41467-024-46812-9.

Eames, M., and T. Kortemme. 2012. "Cost-Benefit Tradeoffs in Engineered Lac Operons." *Science* 336: 911–915. https://doi.org/10.1126/science.1219083.

Ebert, B. E., F. Kurth, M. Grund, L. M. Blank, and A. Schmid. 2011. "Response of *Pseudomonas putida* KT2440 to Increased NADH and ATP Demand." *Applied and Environmental Microbiology* 77: 6597–6605. https://doi.org/10.1128/AEM.05588-11/SUPPL_FILE/AEM05588-11_TABLES4_REV.XLS.

George, K. W., and A. Hay. 2012. "Less Is More: Reduced Catechol Production Permits *Pseudomonas putida* F1 to Grow on Styrene." *Microbiology* 158: 2781–2788. https://doi.org/10.1099/MIC.0.058230-0.

George, K. W., and A. G. Hay. 2011. "Bacterial Strategies for Growth on Aromatic Compounds." *Advances in Applied Microbiology* 74: 1–33. https://doi.org/10.1016/B978-0-12-387022-3.00005-7.

Goormans, A. R., N. Snoeck, H. Decadt, et al. 2020. "Comprehensive Study on *Escherichia coli* Genomic Expression: Does Position Really Matter?" *Metabolic Engineering* 62: 10–19. https://doi.org/10.1016/J.YMBEN.2020.07.007.

Grant, J. R., E. Enns, E. Marinier, et al. 2023. "Proksee: In-Depth Characterization and Visualization of Bacterial Genomes." *Nucleic Acids Research* 51: W484–W492. https://doi.org/10.1093/NAR/GKAD326.

Helsen, J., K. Voordeckers, L. Vanderwaeren, et al. 2020. "Gene Loss Predictably Drives Evolutionary Adaptation." *Molecular Biology and Evolution* 37: 2989–3002. https://doi.org/10.1093/MOLBEV/MSAA172.

Jerison, E. R., A. N. Nguyen Ba, M. M. Desai, and S. Kryazhimskiy. 2020. "Chance and Necessity in the Pleiotropic Consequences of Adaptation for Budding Yeast." *Nature Ecology & Evolution* 4: 601–611. https://doi.org/10.1038/s41559-020-1128-3.

Jimenez, J. I., B. Minambres, J. L. Garcia, and E. Diaz. 2002. "Genomic Analysis of the Aromatic Catabolic Pathways From *Pseudomonas putida* KT2440." *Environmental Microbiology* 4: 824–841. https://doi.org/10.1046/j.1462-2920.2002.00370.x.

Jiménez, J. I., D. Pérez-Pantoja, M. Chavarría, E. Díaz, and V. de Lorenzo. 2014. "A Second Chromosomal Copy of the catA Gene Endows *Pseudomonas putida* Mt-2 With an Enzymatic Safety Valve for Excess of Catechol." *Environmental Microbiology* 16: 1767–1778. https://doi.org/10.1111/1462-2920.12361/SUPPINFO.

Kasai, Y., J. Inoue, and S. Harayama. 2001. "The TOL Plasmid pWW0 xylN Gene Product From *Pseudomonas putida* Is Involved in m-Xylene Uptake." *Journal of Bacteriology* 183: 6662–6666. https://doi.org/10.1128/JB.183.22.6662-6666.2001.

Köbbing, S., T. Lechtenberg, B. Wynands, L. M. Blank, and N. Wierckx. 2024. "Reliable Genomic Integration Sites in *Pseudomonas putida* Identified by Two-Dimensional Transcriptome Analysis." *ACS Synthetic Biology* 13, no. 7: 2060–2072. https://doi.org/10.1021/acssynbio.3c00747.

Kozaeva, E., Z. S. Nielsen, M. Nieto-Domínguez, and P. I. Nikel. 2024. "The pAblo·pCasso Self-Curing Vector Toolset for Unconstrained Cytidine and Adenine Base-Editing in Gram-Negative Bacteria." *Nucleic Acids Research* 52, no. 4: e19. https://doi.org/10.1093/nar/gkad1236.

Lato, D. F., and G. B. Golding. 2020. "Spatial Patterns of Gene Expression in Bacterial Genomes." *Journal of Molecular Evolution* 88: 510–520. https://doi.org/10.1007/S00239-020-09951-3.

Maisnier-Patin, S., and J. R. Roth. 2015. "The Origin of Mutants Under Selection: How Natural Selection Mimics Mutagenesis (Adaptive Mutation)." *Cold Spring Harbor Perspectives in Biology* 7: 1–19. https://doi.org/10.1101/CSHPERSPECT.A018176.

Manoli, M.-T., J. Nogales, and A. Prieto. 2022. "Synthetic Control of Metabolic States in *Pseudomonas putida* by Tuning Polyhydroxyalkanoate Cycle." *MBio* 13, no. 1: e01794. https://doi.org/10.1128/mbio.01794-21.

Martínez-García, E., and V. de Lorenzo. 2011. "Engineering Multiple Genomic Deletions in Gram-Negative Bacteria: Analysis of the Multi-Resistant Antibiotic Profile of *Pseudomonas putida* KT2440." *Environmental Microbiology* 13: 2702–2716. https://doi.org/10.1111/J.1462-2920.2011.02538.X.

Martínez-García, E., and V. de Lorenzo. 2024. "*Pseudomonas putida* as a Synthetic Biology Chassis and a Metabolic Engineering Platform." *Current Opinion in Biotechnology* 85: 103025. https://doi.org/10.1016/J.COPBIO.2023.103025.

Martínez-García, E., S. Fraile, E. Algar, et al. 2023. "SEVA 4.0: An Update of the Standard European Vector Architecture Database for Advanced Analysis and Programming of Bacterial Phenotypes." *Nucleic Acids Research* 51: 13–14. https://doi.org/10.1093/NAR/GKAC1059.

Martínez-García, E., T. Jatsenko, M. Kivisaar, and V. de Lorenzo. 2015. "Freeing *Pseudomonas putida* KT2440 of Its Proviral Load Strengthens Endurance to Environmental Stresses." *Environmental Microbiology* 17: 76–90. https://doi.org/10.1111/1462-2920.12492.

Martin-Pascual, M., C. Batianis, L. Bruinsma, et al. 2021. "A Navigation Guide of Synthetic Biology Tools for *Pseudomonas putida*." *Biotechnology Advances* 49: 107732. https://doi.org/10.1016/J.BIOTECHADV.2021.107732.

Melnyk, A. H., A. Wong, and R. Kassen. 2015. "The Fitness Costs of Antibiotic Resistance Mutations." *Evolutionary Applications* 8: 273–283. https://doi.org/10.1111/EVA.12196.

Moss, E. L., D. G. Maghini, and A. S. Bhatt. 2020. "Complete, Closed Bacterial Genomes From Microbiomes Using Nanopore Sequencing." *Nature Biotechnology* 38: 701–707. https://doi.org/10.1038/s41587-020-0422-6.

Muñoz, R., L. F. Díaz, S. Bordel, and S. Villaverde. 2007. "Inhibitory Effects of Catechol Accumulation on Benzene Biodegradation in *Pseudomonas Putida* F1 Cultures." *Chemosphere* 68: 244–252. https://doi.org/10.1016/J.CHEMOSPHERE.2007.01.016.

Navarre, W. W., M. McClelland, S. J. Libby, and F. C. Fang. 2007. "Silencing of Xenogeneic DNA by H-NS—Facilitation of Lateral Gene Transfer in Bacteria by a Defense System That Recognizes Foreign DNA." *Genes & Development* 21: 1456–1471. https://doi.org/10.1101/gad.1543107.

Nikel, P. I., and V. de Lorenzo. 2018. "*Pseudomonas putida* as a Functional Chassis for Industrial Biocatalysis: From Native Biochemistry to Trans-Metabolism." *Metabolic Engineering* 50: 142–155. https://doi.org/10.1016/j.ymben.2018.05.005.

Nikel, P. I., E. Martínez-García, and V. de Lorenzo. 2014. "Biotechnological Domestication of Pseudomonads Using Synthetic Biology." *Nature Reviews Microbiology* 12, no. 5: 368–379. https://doi.org/10.1038/nrmicro3253.

Nogales, J., J. Mueller, S. Gudmundsson, et al. 2020. "High-Quality Genome-Scale Metabolic Modelling of *Pseudomonas putida* Highlights Its Broad Metabolic Capabilities." *Environmental Microbiology* 22, no. 1: 255–269. https://doi.org/10.1111/1462-2920.14843.

Panke, S., J. M. Sánchez-Romero, and V. de Lorenzo. 1998. "Engineering of Quasi-Natural *Pseudomonas putida* Strains Toluene Metabolism Through an Ortho-Cleavage Degradation Pathway." *Applied and Environmental Microbiology* 64: 748–751. https://doi.org/10.1128/aem.64.2.748-751.1998.

Qin, L., A. M. Erkelens, F. Ben Bdira, and R. T. Dame. 2019. "The Architects of Bacterial DNA Bridges: A Structurally and Functionally Conserved Family of Proteins." *Open Biology* 9: 190223. https://doi.org/10.1098/rsob.190223.

Quesada, J. M., M. I. Soriano, and M. Espinosa-Urgel. 2012. "Stability of a *Pseudomonas putida* KT2440 Bacteriophage-Carried Genomic Island and Its Impact on Rhizosphere Fitness." *Applied and Environmental Microbiology* 78: 6963–6974. https://doi.org/10.1128/AEM.00901-12.

Ramos, J. L., M. S. Cuenca, C. Molina-Santiago, et al. 2015. "Mechanisms of Solvent Resistance Mediated by Interplay of Cellular Factors in *Pseudomonas putida*." *FEMS Microbiology Reviews* 39: 555–566. https://doi.org/10.1093/FEMSRE/FUV006.

Ray, P., V. Girard, M. Gault, et al. 2012. "*Pseudomonas putida* KT2440 Response to Nickel or Cobalt Induced Stress by Quantitative Proteomics†." *Metallomics* 5, no. 1: 68–79.

Reams, A. B., and J. R. Roth. 2015. "Mechanisms of Gene Duplication and Amplification." *Cold Spring Harbor Perspectives in Biology* 7, no. 2: a016592. https://doi.org/10.1101/CSHPERSPECT.A016592.

Regenhardt, D., H. Heuer, S. Heim, et al. 2002. "Pedigree and Taxonomic Credentials of *Pseudomonas putida* Strain KT2440." *Environmental Microbiology* 4: 912–915. https://doi.org/10.1046/j.1462-2920.2002.00368.x.

Renzi, F., E. Rescalli, E. Galli, and G. Bertoni. 2010. "Identification of Genes Regulated by the MvaT-Like Paralogues TurA and TurB of *Pseudomonas putida* KT2440." *Environmental Microbiology* 12: 254–263. https://doi.org/10.1111/j.1462-2920.2009.02064.x.

Sauer, C., S. Syvertsson, L. C. Bohorquez, et al. 2016. "Effect of Genome Position on Heterologous Gene Expression in *Bacillus subtilis*: An Unbiased Analysis." *ACS Synthetic Biology* 5: 942–947. https://doi.org/10.1021/acssynbio.6b00065.

Sauer, U. 2001. "Evolutionary Engineering of Industrially Important Microbial Phenotypes." *Advances in Biochemical Engineering/Biotechnology* 73: 129–169. https://doi.org/10.1007/3-540-45300-8_7.

Scholz, S. A., C. D. Lindeboom, and P. L. Freddolino. 2022. "Genetic Context Effects Can Override Canonical Cis Regulatory Elements in *Escherichia coli*." *Nucleic Acids Research* 50: 10360–10375. https://doi.org/10.1093/nar/gkac787.

Shen, B. A., and R. Landick. 2019. "Transcription of Bacterial Chromatin." *Journal of Molecular Biology* 431: 4040–4066. https://doi.org/10.1016/J.JMB.2019.05.041.

Tas, H., L. Grozinger, R. Stoof, V. de Lorenzo, and Á. Goñi-Moreno. 2021. "Contextual Dependencies Expand the Re-Usability of Genetic Inverters." *Nature Communications* 12, no. 1: 1–9. https://doi.org/10.1038/s41467-020-20656-5.

Torres-Bacete, J., J. Luís García, and J. Nogales. 2021. "A Portable Library of Phosphate-Depletion Based Synthetic Promoters for Customable and Automata Control of Gene Expression in Bacteria." *Microbial Biotechnology* 14, no. 6: 2643–2658. https://doi.org/10.1111/1751-7915.13808.

van der Meer, J. R., W. M. de Vos, S. Harayama, and A. J. Zehnder. 1992. "Molecular Mechanisms of Genetic Adaptation to Xenobiotic Compounds." *Microbiological Reviews* 56: 677–694. https://doi.org/10.1128/MR.56.4.677-694.1992.

Weimer, A., M. Kohlstedt, D. C. Volke, P. I. Nikel, and C. Wittmann. 2020. "Industrial Biotechnology of *Pseudomonas Putida*: Advances and Prospects." *Applied Microbiology and Biotechnology* 104: 7745–7766. https://doi.org/10.1007/S00253-020-10811-9.

Weinel, C., K. E. Nelson, and B. Tümmler. 2002. "Global Features of the *Pseudomonas putida* KT2440 Genome Sequence." *Environmental Microbiology* 4: 809–818. https://doi.org/10.1046/j.1462-2920.2002.00331.x.

Williams, P. A., L. M. Shaw, C. W. Pitt, and M. Vrecl. 1997. "xyIUW, Two Genes at the Start of the Upper Pathway Operon of TOL Plasmid pWW0, Appear to Play no Essential Part in Determining Its Catabolic Phenotype." *Microbiology* 143: 101–107. https://doi.org/10.1099/00221287-143-1-101.

Worsey, M. J., and A. P. Williams. 1975. "Metablism of Toluene and Xylenes by *Pseudomonas putida* (Arvilla) mt 2: Evidence for a New Function of the TOL Plasmid." *Journal of Bacteriology* 124: 7–13. https://doi.org/10.1128/jb.124.1.7-13.1975.

Zobel, S., I. Benedetti, L. Eisenbach, V. de Lorenzo, N. Wierckx, and L. M. Blank. 2015. "Tn7-Based Device for Calibrated Heterologous Gene Expression in *Pseudomonas putida*." *ACS Synthetic Biology* 4: 1341–1351. https://doi.org/10.1021/ACSSYNBIO.5B00058/SUPPL_FILE/SB5B00058_SI_001.XLSX.

Supporting Information

Additional supporting information can be found online in the Supporting Information section.